Journal of Solid State Chemistry 184 (2011) 2150–2158

Contents lists available at ScienceDirect

Journal of Solid State Chemistry

journal homepage: www.elsevier.com/locate/jssc

Seed-mediated synthesis, properties and application of γ-Fe_2O_3–CdSe magnetic quantum dots

Alex W.H. Lin [a], Chung Yen Ang [a], Pranab K. Patra [a], Yu Han [a], Hongwei Gu [a], Jean-Marie Le Breton [b,*], Jean Juraszek [b], Hubert Chiron [b], Georgia C. Papaefthymiou [c], Subramanian Tamil Selvan [a,**,1], Jackie Y. Ying [a,***]

[a] Institute of Bioengineering and Nanotechnology, 31 Biopolis Way, The Nanos, Singapore 138669, Singapore
[b] Groupe de Physique des Matériaux, UMR 6634 CNRS, Université de Rouen, Site Universitaire du Madrillet, Avenue de l'Université, BP 12 76801 Saint Etienne du Rouvray Cedex, France
[c] Department of Physics, Villanova University, Villanova, PA 19085, USA

ARTICLE INFO

Article history:
Received 2 February 2011
Received in revised form
17 April 2011
Accepted 29 May 2011
Available online 6 June 2011

Keywords:
Magnetic quantum dots
Seed-mediated growth
Superparamagnetism

ABSTRACT

Seed-mediated growth of fluorescent CdSe quantum dots (QDs) around γ-Fe_2O_3 magnetic cores was performed at high temperature (300 °C) in the presence of organic surfactants. Bi-functional magnetic quantum dots (MQDs) with tunable emission properties were successfully prepared. The as-synthesized MQDs were characterized by high-resolution transmission electron microscopy (HRTEM) and dynamic light scattering (DLS), which confirmed the assembly of heterodimers. When a longer growth period was employed, a homogeneous dispersion of QDs around a magnetic nanoparticle was obtained. The magnetic properties of these nanocomposites were examined. The MQDs were superparamagnetic with a saturation magnetization of 0.40 emu/g and a coercivity of 138 Oe at 5 K. To demonstrate their potential application in bio-labeling, these MQDs were coated with a thin silica shell, and functionalized with a polyethylene glycol (PEG) derivative. The functionalized MQDs were effectively used for the labeling of live cell membranes of 4T1 mouse breast cancer cells and HepG2 human liver cancer cells.

1. Introduction

The chemically synthesized II–VI semiconductor nanocrystals, also known as quantum dots (QDs), exhibit size-dependent optical properties such as sharp, tunable emission, broad absorption, single source excitation, and long-term photostability. These interesting optical properties have enabled the QDs to be used in applications ranging from electronics [1,2] to biology [3–6]. On the other hand, magnetic nanoparticles (MPs) have been increasingly employed in magnetic resonance imaging (MRI) as contrast agents [7–11], MR tracking of dendritic cells for cellular therapy [12], hyperthermia [13], and nanomedicine platforms in drug delivery [14]. Recently, Cheon and coworkers have shown an enhanced MRI sensitivity for the detection of cancer markers using artificially engineered MPs [15].

Our interest lies in combining QDs and MPs in a single nanocomposite system [16]. The resulting bi-functional materials – magnetic quantum dots (MQDs) [17,18] – would be useful for both fluorescence-based cell labeling and magnetically based cell separation, drug targeting and MRI applications. Hence, there is a great interest on the synthesis and characterization of this new class of nanocomposites, as in general with the development of nanocrystalline materials [19].

The synthesis, properties, and perspectives of hybrid nanocrystal structures have been recently reviewed [20,21]. The examples for heterodimers include magnetic semiconductors (e.g. FePt–CdS [22], γ-Fe_2O_3–CdS [23], γ-Fe_2O_3–ZnS [23], and γ-Fe_2O_3–TiO_2 nanorods [24,25]), magnetic noble metal systems (e.g. $CoPt_3$–Au [26,27], Fe_3O_4–Au [28a], Fe_3O_4–Ag [28a,b] and FePt–Ag [29]), and bimetallic nanoparticles (e.g. Au–Ag [29]). Gu et al. [22] demonstrated an interesting approach to the fabrication of heterodimers consisting of FePt–CdS through an organometallic approach. Klimov and coworkers have also shown that Co–CdSe core-shell nanocomposites could be prepared by the drop-wise addition of CdSe precursors into a vigorously stirred mixture of Co nanocrystals and surfactants (trioctylphosphine oxide (TOPO) and hexadecyl amine (HDA)) at 140 °C for overnight growth [30]. Although these two systems were bi-functional, their fluorescence quantum yield was low (<4%).

* Corresponding author. Fax: +33 0 232955032.
** Corresponding author. Fax: +65 67744657.
*** Corresponding author. Fax: +65 64789020.
E-mail addresses: jean-marie.lebreton@univ-rouen.fr (J.-M. Le Breton), subramaniant@imre.a-star.edu.sg (S. Tamil Selvan), jyying@ibn.a-star.edu.sg (J.Y. Ying).
[1] Present address: Institute of Materials Research and Engineering, 3 Research Link, Singapore 117602, Singapore.

0022-4596/$ - see front matter © 2011 Elsevier Inc. All rights reserved.
doi:10.1016/j.jssc.2011.05.043

The over-coating of CdSe with a higher band gap material (ZnS) for these nanocomposites has not been reported. Deka and coworkers [31] developed a colloidal two-step seeded-growth approach to synthesize three-component magnetic/semiconductor hybrid nanocrystals consisting of single-metallic Co head connected to either apexes of CdSe–CdS core-shell nanorods. The nanocrystals retained appreciable fluorescence in spite of photoexcited charge transfer from the semiconductor to the metal domain, and exhibited unusual ferromagnetic-like behavior at room temperature. Di Corato and coworkers [32] prepared spherical nanobeads by grafting fluorescent oligothiophene molecules to an amphiphilic polymer that was used to enwrap magnetic iron oxide nanoparticles. Such nanostructures displaying fluorescence and magnetic properties at the same time are potentially useful for magnetic separation and multiplexed optical detection of different tumor cell populations.

We have shown that the QDs and MPs synthesized separately could be incorporated within silica by a facile reverse microemulsion method [16]. The resulting nanocomposites displayed the emission and magnetic properties characteristic of QDs and MPs, respectively. However, they showed low quantum yield and required long synthesis time. We have also reported briefly on the seed-mediated synthesis of MQDs by growing CdSe QDs on Fe_2O_3 cores, yielding either heterodimers or a homogeneous dispersion of QDs around Fe_2O_3. This method allowed for flexibility in tuning the optical and magnetic properties separately [33]. We have further demonstrated the silica coating of hydrophobic QDs (e.g. CdSe, ZnS–CdSe [34], and PbSe [35]) and MQDs in a reverse microemulsion.

This paper presents the detailed synthesis, structural, optical and magnetic properties of seed-mediated synthesis of MQDs. The MQDs were coated with a thin silica layer via the reverse microemulsion method, and surface functionalized with a PEG derivative [36] consisting of oleyl groups at one end and NHS ester at the other end to allow for the specific labeling of live cells' membranes.

2. Experimental

Materials: iron pentacarbonyl ($Fe(CO)_5$, 99.999%), octyl ether (99%), oleic acid (99%), cadmium oxide (CdO, 99%), stearic acid (95%), TOPO (99%), HDA (99%), trioctylphosphine (TOP, 90% tech), Se (99.5%, 100 mesh) were purchased from Sigma-Aldrich. All syntheses were performed in air-free Schlenk line setup in argon.

Synthesis of γ-Fe_2O_3 MPs: the synthesis of maghemite nanoparticles was based on literature protocols [37]. Typically, a mixture containing $Fe(CO)_5$ (0.2 mL, 1.52 mmol), octyl ether (10 mL), oleic acid (1.28 g, 4.56 mmol) was heated at 100 °C. The temperature was slowly raised to reflux (~280 °C) and maintained for 1 h. The resulting black solution was cooled, and an oxidant ($(CH_3)_3NO$, 0.34 g) was added. The mixture was then heated to 130 °C and kept for 2 h. After cooling to room temperature, the growth solution was precipitated with ethanol. The MPs were collected by centrifugation, washed with ethanol (3 ×) and vacuum dried at 80 °C.

Synthesis of γ-Fe_2O_3–CdSe MQDs: Peng and coworkers have developed CdO-based synthesis of CdSe QDs using TOPO and HDA as surfactants [38,39]. We followed a similar route with the same surfactants for CdSe synthesis. In preparing the MQDs, CdO (0.05 g, 0.39 mmol) and stearic acid (0.456 g) were first heated to 150–200 °C, and then cooled to room temperature. MPs (0.025 g, 0.156 mmol), TOPO (7.76 g) and HDA (7.76 g) were added to this mixture, which was then heated to 280–300 °C. Se (0.32 g, 4 mmol) dissolved in 9.6 mL of TOP was quickly injected into this mixture within a few seconds, and the resulting CdSe QDs were allowed to grow for different time periods (1–5 min) to yield different dot sizes that corresponded to green, yellow, orange and red emissions. The aliquots of growth solution were quenched by the addition of chloroform. Methanol was then added to the growth solution, and a magnet was applied to the sample vial. All the particles were attracted to the magnet, leaving behind a clear solution. The harvested particles were both magnetic and fluorescent, confirming the successful synthesis of MQD nanocomposite particles.

Silica coating of MQDs: MQDs passivated with TOPO/HDA were precipitated once with methanol, and the precipitate was dried under normal conditions at room temperature. 4 mg of the precipitated MQDs was dispersed in 1 mL of chloroform. Micelles were prepared by dissolving 0.2 g of Igepal-CO520 (polyoxyethylene(5)nonylphenyl ether) in 4 mL of cyclohexane, and stirring vigorously for 30 min. The MQDs in chloroform were added to the micelles along with 10–50 μL of aminopropyl trimethoxysilane (APS), and the mixture was stirred for 1 h. Next, 5–20 μL of tetramethyl ammonium hydroxide (TMAH) in 2-propanol/methanol was added to the mixture. After 1 h of stirring, 20 μL of deionized water was added. The mixture was stirred for another 30 min until the bulk organic phase turned colorless, with the

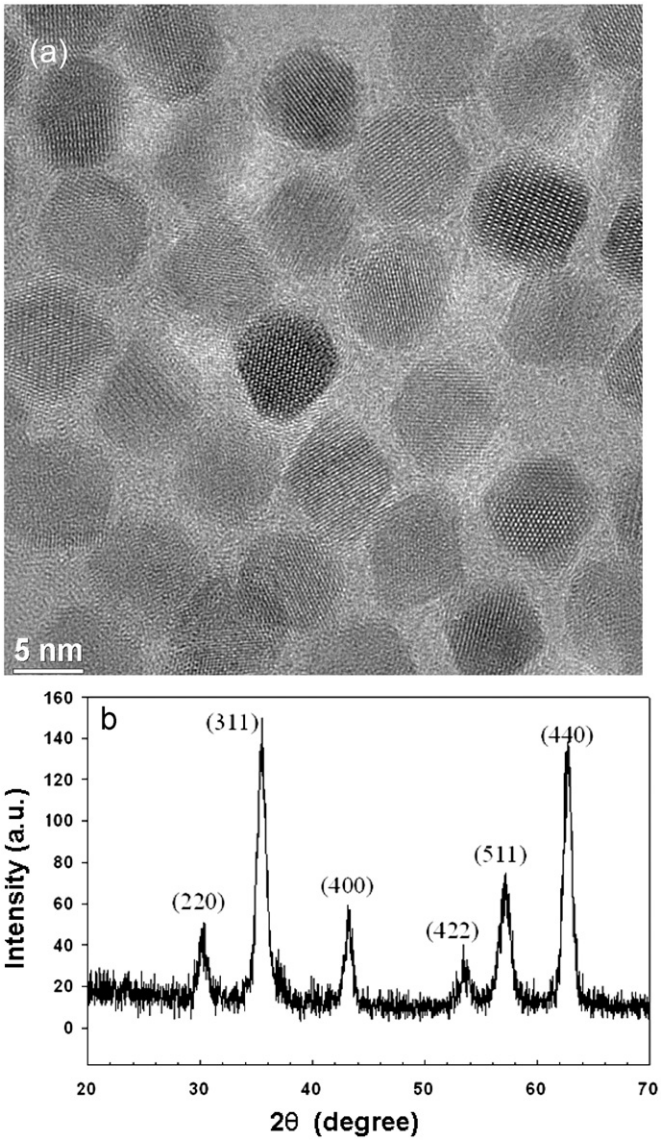

Fig. 1. (a) HRTEM image of oleic acid capped MPs. The size of MPs ranges from 8 to 10 nm. (b) XRD pattern of γ-Fe_2O_3 MPs.

formation of orange/red globules on the surface of the glass vial. The colorless organic phase was then discarded, leaving behind the silica-coated MQDs (SiO_2/MQDs) on the surface of the glass vial. The SiO_2/MQDs were washed with chloroform 3–5 times to ensure the complete removal of excess surfactants and other unreacted reagents from their surface. They were then dispersed in 1 mL of 1 × phosphate buffered saline (PBS), and used immediately for bioconjugation to prevent precipitation. The second addition of 10–50 μL of APS improved the stability of the SiO_2/MQDs in buffer.

Bioconjugation of SiO_2/MQDs: the silanized MQDs were conjugated to oleyl-O-poly(ethyleneglycol)-succinyl-N-hydroxysuccinimidyl ester, denoted as bio-anchored membrane (BAM) [36], which was purchased from NOF Corporation, Tokyo. We devised two methods of conjugating BAM with SiO_2/MQDs. Both bioconjugation methods were found to be effective. In the first method, 10 mg of BAM was added to SiO_2/MQDs (4 mg/mL) in buffer. The NHS ester of BAM could readily react with the surface amine groups of SiO_2/MQDs to form an amide linkage between the BAM and the MQDs. In the second method, 10 mg of BAM was dissolved in 1 mL of anhydrous dichloromethane, and 10–50 μL of APS were added. The mixture was allowed to react for 1 h with stirring. The solvent was evaporated, and the residue was dissolved in 1 mL of aqueous dispersion of SiO_2/MQDs. The surface silanol groups on the silica-coated particles were reacted with the APS conjugated to BAM. The final aqueous solution was filtered through a 0.2-μm filter to remove any large aggregates.

Culture and labeling of mammalian cells: two adherent cell lines, HepG2 human liver cancer cells and 4T1 mouse breast cancer cells, were used for bioimaging. HepG2 cells were propagated in Dulbecco's modified Eagle's medium (DMEM) supplemented with 10% fetal bovine serum (FBS) and 1% penicillin/streptomycin; while 4T1 cells were cultured in Roswell Park Memorial Institute's medium (RPMI-1630). All cells were pre-cultured overnight at a density of 0.2 million cells/mL on a 10-mm cover slip at 37 °C and 5% of CO_2. 50–100 μL of BAM/SiO_2/MQDs were loaded onto the cells, and incubated for at least 5 min.

Instrumentation: An FEI Technai G2 high-resolution transmission electron microscope was used to image the MQDs. Absorption and emission spectra were acquired with UV–vis-NIR spectrophotometer (UV-3600 Shimadzu) and Fluorolog (FL 3–11) fluorometer, respectively. DLS experiments were performed with Brookhaven 05-LHP-928 laser light scattering system (He-Ne laser, 35 mW). Quantum yields were estimated by comparing the integrated emission intensity of QDs or MQDs to that of an organic dye (Rhodamine 6G) at the same optical density (0.1) and excitation wavelength (365 nm) using the following equation:

$$QY = \left(\frac{abs_{Std}}{abs_X}\right)\left(\frac{\Delta\Phi_X}{\Delta\Phi_{Std}}\right)q_{Std}$$

where QY is the quantum yield of sample, abs_{Std} is absorbance of dye=0.1, abs_X is absorbance of sample, $\Delta\Phi_X$ is integrated area under the emission spectrum of sample, $\Delta\Phi_{Std}$ is integrated area under the emission spectrum of dye, and q_{Std} is quantum yield of dye=95%.

The magnetic properties of the γ-Fe_2O_3–CdSe MQDs were recorded using a SQUID magnetometer (Quantum Design MPMS XL). The sample mass used for the measurements was 6.5 mg. Confocal laser scanning microscope (CLSM) (Olympus Fluoview 300 confocal microscope) was used to observe the cell labeling.

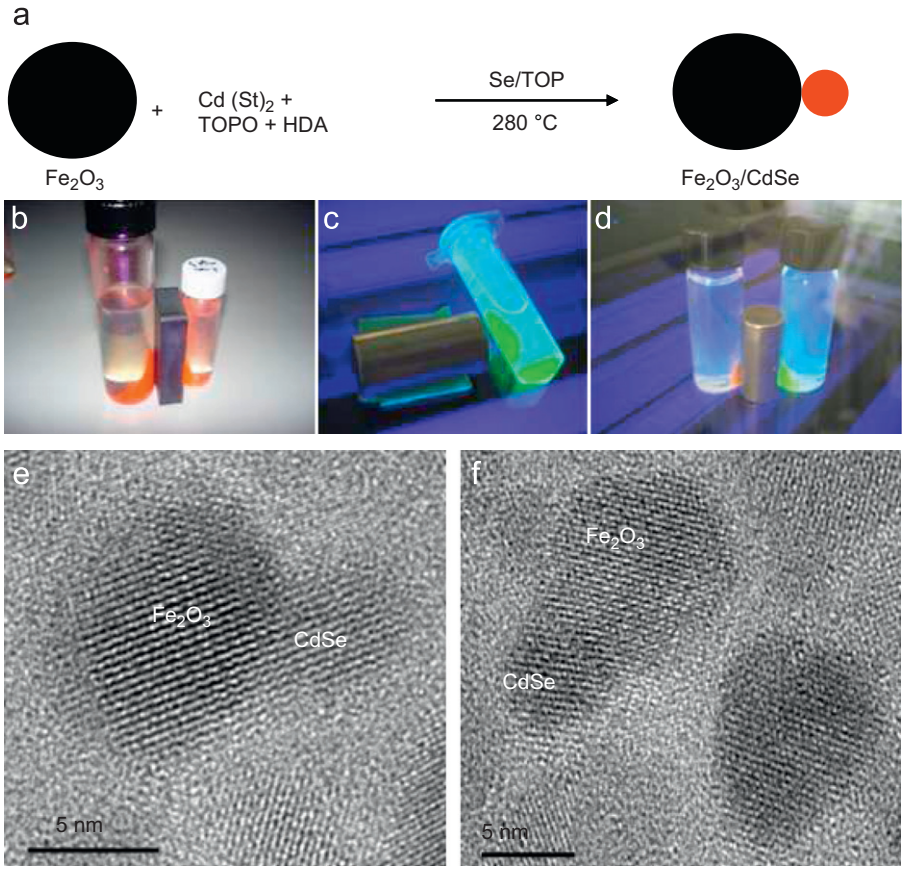

Fig. 2. (a) Schematic of the formation of γ-Fe_2O_3–CdSe MQDs, (b–d) photographs showing the fluorescence and magnetic properties of MQDs after magnetic harvesting and excitation at 365 nm (by UV lamp), and (e, f) HRTEM images of γ-Fe_2O_3–CdSe MQD dimers (11–14 nm).

3. Results and discussion

3.1. TEM analysis of γ-Fe_2O_3–CdSe MQDs

The size of as-synthesized γ-Fe_2O_3 MPs was 8–10 nm (Fig. 1a). The MPs were coated with oleic acid in the synthesis following literature protocols [37]. Most of the particles were octahedral, and some of them were spherical in morphology. The HRTEM image confirmed the highly crystalline nature of the particles (Fig. 1a). Fig. 1b shows the X-ray diffraction (XRD) pattern of the MPs, which corresponded to the maghemite (γ-Fe_2O_3) phase [37].

In fabricating MQDs, CdSe QDs were grown onto γ-Fe_2O_3 magnetic cores (Scheme in Fig. 2a). The addition of methanol destabilized the growth solution and caused the particles to precipitate. The particles were harvested by a magnet, leaving behind a colorless supernatant. Fig. 2b–d shows the fluorescence (excitation wavelength = 365 nm) and magnetic properties of the harvested particles. The supernatant was not fluorescent, indicating the absence of QDs. The harvested particles were dispersed in chloroform and precipitated with methanol, and a magnet was applied to harvest the particles. The cycle of precipitation and re-dispersion was repeated at least three times to ensure that all free QDs were removed. The HRTEM images (Fig. 2e and f) indicated that the γ-Fe_2O_3–CdSe particles synthesized at short growth times (1–2 min) were assembled as heterodimers. The fusing of the crystal lattices of γ-Fe_2O_3 MP and CdSe QD in the heterodimers was clearly seen. Fig. 3 illustrates that a small quantity ($< 5\%$) of trimers was also present. The overall size of MQDs ranged from 11 to 14 nm.

The mechanism of heterodimer formation has been proposed by several groups [20–23]. The formation of heterodimers is dependent on the lattice match/mismatch between the crystal lattices of two different materials. In a core-shell structure, the growth of the shell material is dependent on the lower injection temperature and slower addition of precursors, and on the partial miscibility of the two materials. The interfacial energy also plays an important role in directing the formation of heterostructures. The three dominant mechanisms for the formation of heterodimers include: (1) phase segregation of two immiscible materials, (2) coalescence of an initially formed amorphous shell, and (3) seed-mediated selective nucleation and growth. The first mechanism would be applicable when the interfacial energy is large enough between the two materials, resulting in the phase segregation of two separate particle domains (e.g. Co–Pd and Cu–In sulfide heterodimers) [20,21]. In the second mechanism, a shell is first formed around the seed nanoclusters at a sufficiently low interfacial energy [21]. Upon annealing, the amorphous shell can be crystallized. The third mechanism applies to the synthesis reported herein.

Specifically, our dimers were formed by seed-mediated nucleation and growth of QDs on the core γ-Fe_2O_3 MPs. This was in agreement with a similar mechanism proposed for CoPt–Au by Pellegrino et al. [27]. In another recent study, it was shown that

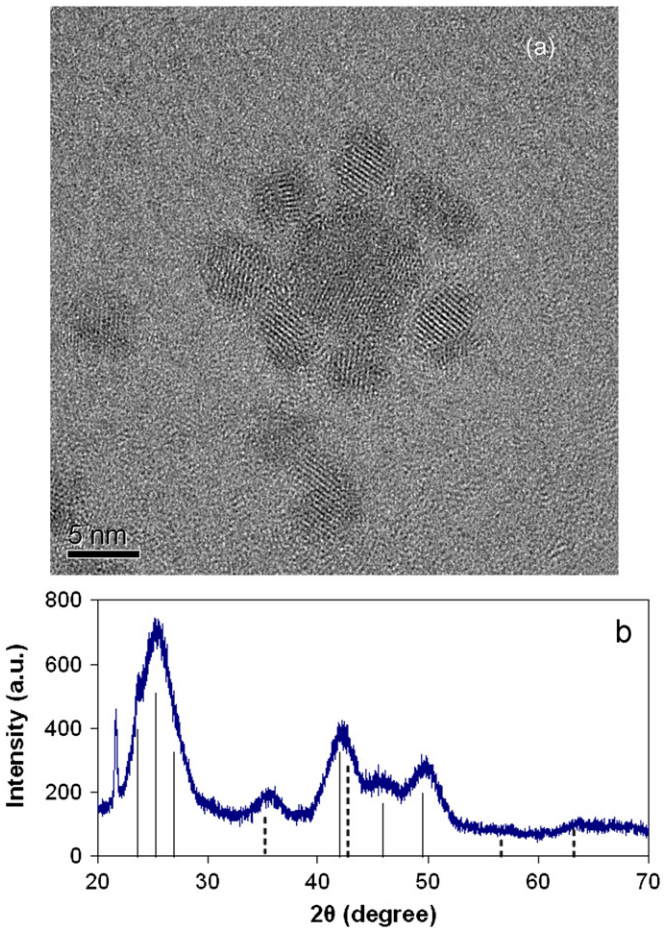

Fig. 4. (a) HRTEM image of MQDs showing the assembly of QDs around a MP. The QDs (4–5 nm) were grown at 280 °C for 5 min. (b) XRD pattern of MQDs. The vertical solid and dotted lines correspond to the wurtzite structure of CdSe and γ-Fe_2O_3, respectively.

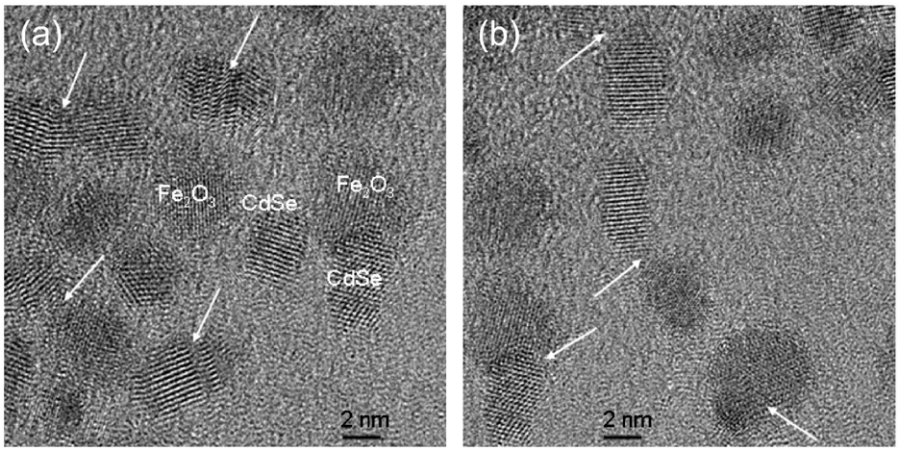

Fig. 3. (a, b) HRTEM images of γ-Fe_2O_3–CdSe MQDs, which are mostly assembled as dimers (11–14 nm). The arrows indicate the intersection of QDs and MPs.

γ-Fe_2O_3 and II–VI QDs (e.g. CdS) exhibited a substantial lattice mismatch, and therefore composed of both dimers and isolated particles [23]. In preparing the dimers, we have taken extensive care to remove the free QDs by magnetic precipitation and re-dispersion cycles. In some cases, centrifugation at a low speed (1000 rpm) was employed to precipitate the MQDs, leaving behind free QDs in the supernatant. Hydrophobic–hydrophobic interactions were the main factor for the formation of bi-functional MQDs. When methanol was added, both the MPs and QDs were believed to be aggregated and separated by the magnet, due to either the presence of dimers or the formation of the hydrophobic bilayer, utilizing the interaction of the surfactants (oleic acid on the MP surface and TOPO/HDA on the QD surface). After dispersion of the precipitate in chloroform, surfactants kept the MQDs highly dispersed in the system. Heterodimers were formed at shorter growth period (1–3 min, corresponding to green and yellow emissions) (see Fig. 2e and f). Interestingly, after a longer growth period (5–8 min, corresponding to orange and red emissions), an assembly of QDs was found around the MPs, although a gap existed between the QDs and MPs (Fig. 4a). Thus, we hypothesized that heterodimers were formed at shorter growth periods, whereas trimers and tetramers might result at longer growth periods, leading to a crown of QDs (homogeneous dispersion of QDs) around the MP cores. At first, QDs would nucleate closer to the MPs (cores), resulting in dimers. Once the nucleation sites were occupied by QDs (dimers, trimers, etc.), then QDs would nucleate on their own, resulting in individual particles.

The XRD pattern of MQDs is shown in Fig. 4b. The peaks at $2\theta \sim 23.7^\circ$, 25.5°, 27°, 42.4°, 45.5°, and 49.8° corresponded to the wurtzite structure of CdSe, and the peaks at $2\theta \sim 35.6^\circ$, 43.5°, 57.1°, and 62.7° corresponded to γ-Fe_2O_3 MPs. The selected area electron diffraction pattern displayed the rings that originated from the wurtzite structure of CdSe and the maghemite phase of Fe_2O_3. The energy dispersive X-ray (EDX) analysis of the heterodimers further confirmed that the darker and lighter regions mainly consisted of Fe, and Cd and Se, respectively. This was in good agreement with the diffraction pattern reported for Fe_3O_4–CdSe heterodimers [40].

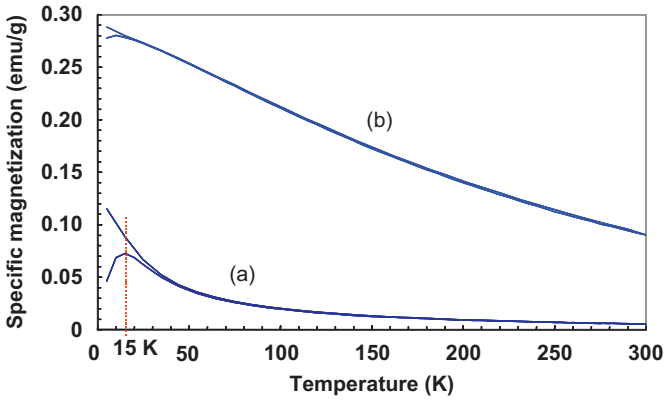

Fig. 6. ZFC/FC magnetization curves of γ-Fe_2O_3–CdSe MQDs under an applied field of (a) 50 Oe and (b) 1000 Oe.

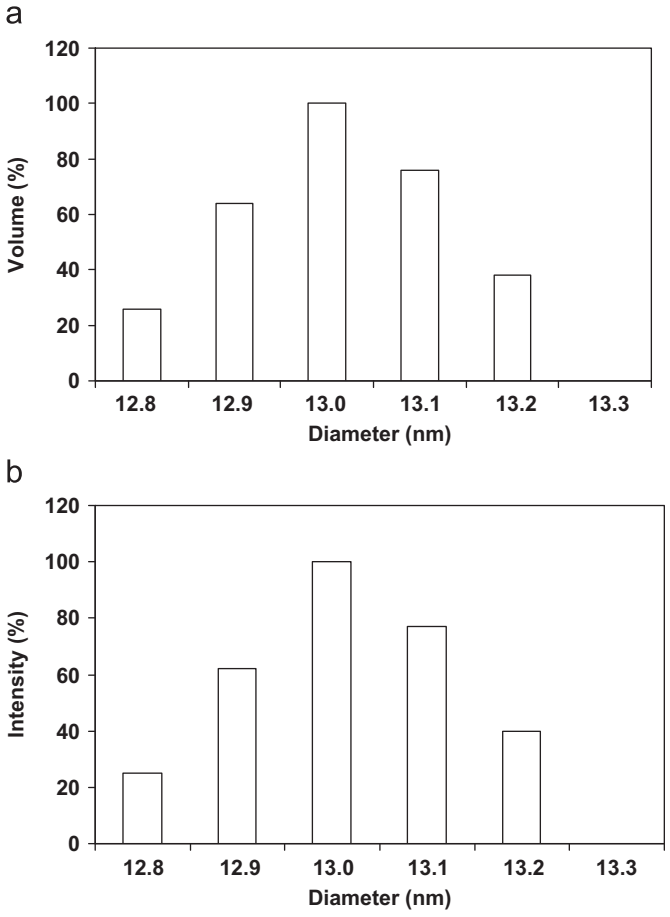

Fig. 5. (a) Volume- and (b) intensity-weighted particle size distribution of γ-Fe_2O_3–CdSe MQDs synthesized at 280 °C with a growth period of 3 min, obtained from DLS experiments. The mean diameter of heterodimers is 13 nm.

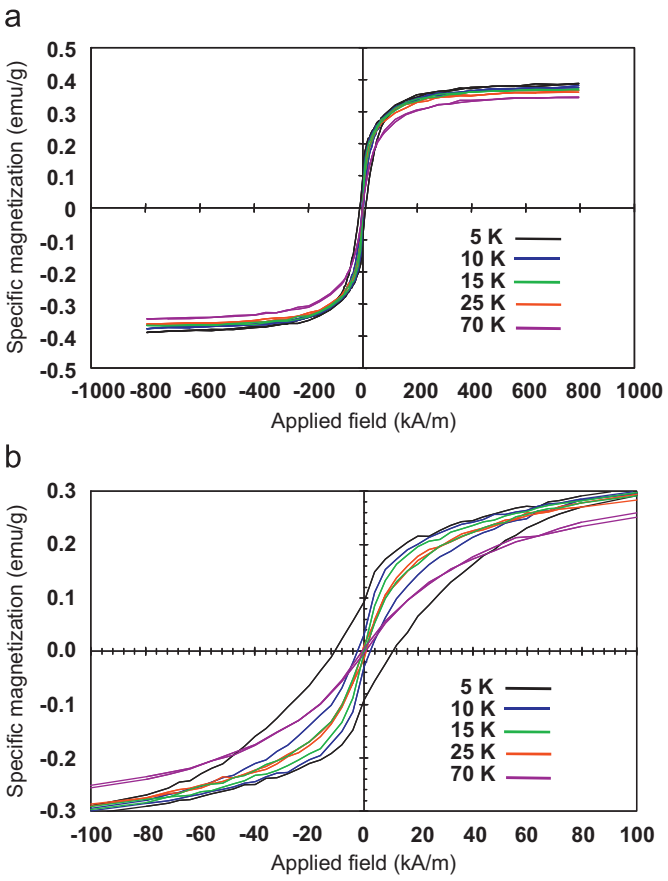

Fig. 7. (a) Full hysteresis loops of γ-Fe_2O_3–CdSe MQDs at temperatures below and above the blocking temperature. (b) Expanded hysteresis loops showing clearly the dependence of the coercive field on temperature, and the collapse of the hysteresis loop above the blocking temperature.

3.2. DLS analysis of MQDs

Before the analysis, 3 mL of MQD samples were filtered ~10 times with 0.2-μm filter to ensure that the samples were of high quality (i.e. free from dust particles and particle agglomerates). DLS data indicated that most of the particles were dimers with an overall size of 12–14 nm, depending on the size of QDs grown by varying the growth period (1–5 min) in the synthesis. A typical example is illustrated in Fig. 5. The particle sizes derived from DLS analysis were comparable to those obtained from TEM.

3.3. Magnetic properties of γ-Fe_2O_3–CdSe MQDs

The magnetic properties of as-harvested MQDs were investigated using SQUID magnetometry. The zero-field-cooled (ZFC) and field-cooled (FC) curves obtained under two different applied fields (50 and 1000 Oe) are shown in Fig. 6. The superparamagnetic behavior was clearly observed. The ZFC curve exhibited a maximum at 15 K under an applied field of 50 Oe. The magnetic particles were in the blocked state at a low temperature (5 K), with the magnetic moments of the particles (or macro-spins) being randomly oriented in the sample. As the temperature increased, the macro-spins were progressively unblocked due to the increase in thermal energy, and immediately aligned in the direction of the applied field. This induced an increase in the magnetization of the sample up to 15 K. At higher temperatures, thermal energy induced fast fluctuations or reversals of the macro-spins and concomitant decrease in magnetization. The low temperature of the observed maximum was indicative of the relatively small magnetic anisotropy energy, while the sharpness of the peak reflected a narrow MP size distribution in the sample. The ZFC/FC curves obtained at 1000 Oe revealed the same effect, but the maximum of the ZFC peak was less pronounced. When the applied field was too high, the macro-spins were aligned in the direction of the applied field even at very low temperatures, and the blocking phenomenon could not be observed.

The observed superparamagnetic behavior, characteristic of small magnetically ordered structures [41,42], was due to the

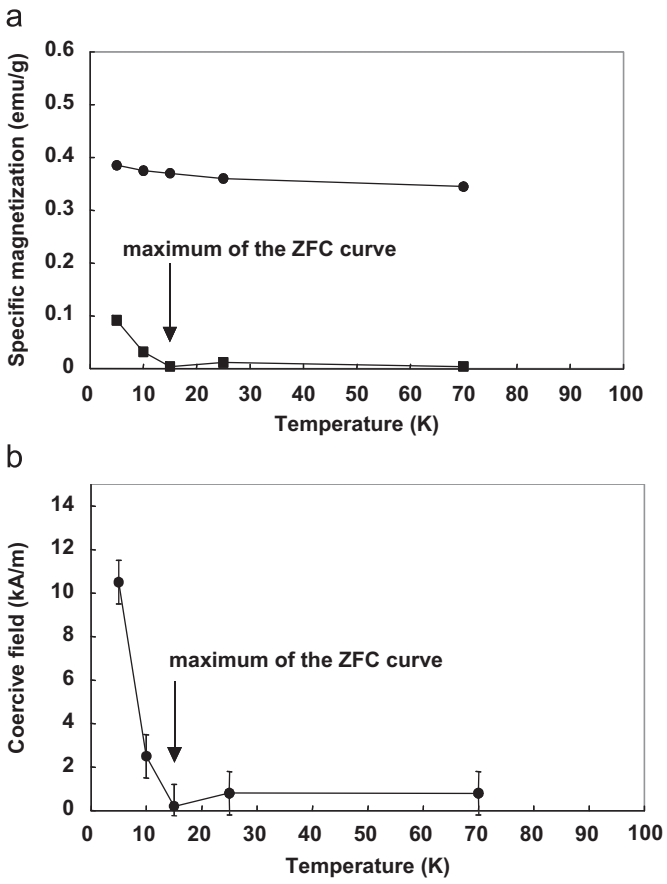

Fig. 8. Temperature dependence of γ-Fe_2O_3–CdSe MQDs on the (a) (●) saturation and (■) remnant magnetizations, and (b) coercive field.

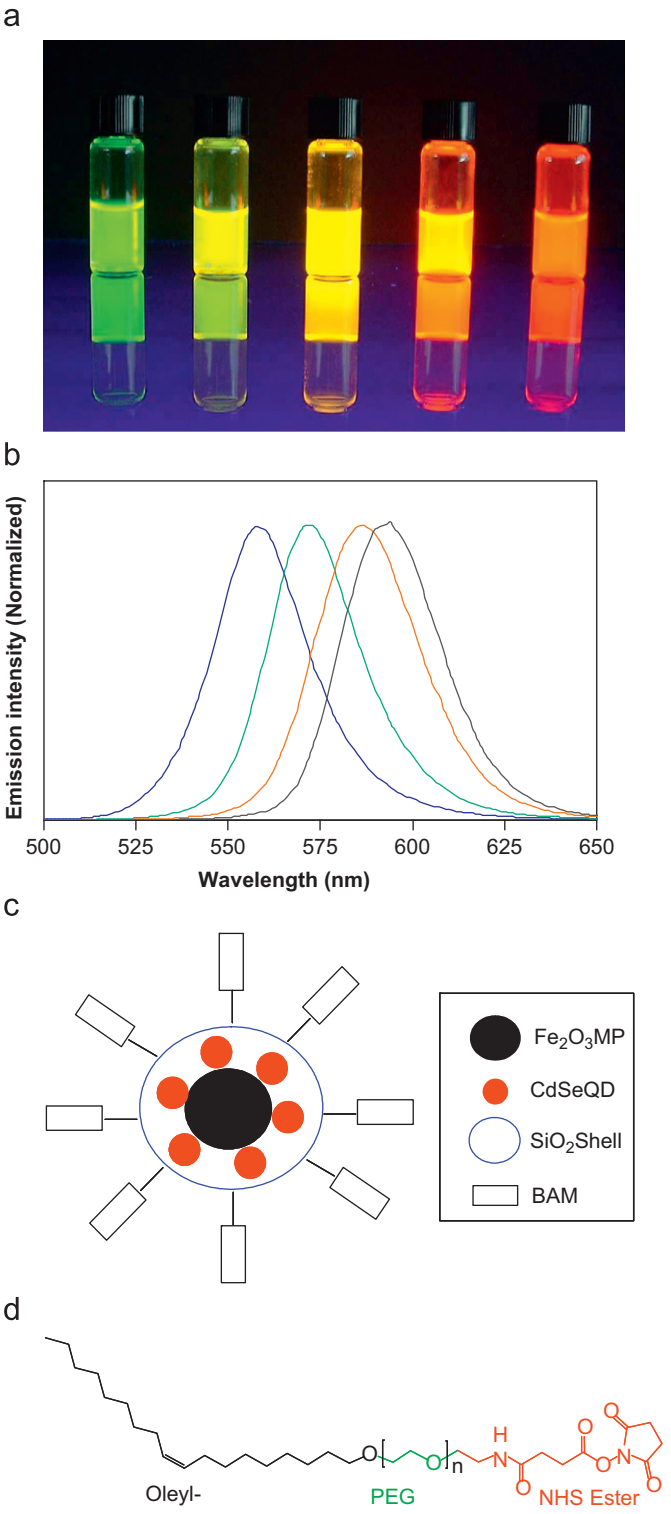

Fig. 9. (a) Photograph showing the emission of SiO_2/MQDs in buffer. Excitation wavelength = 365 nm. (b) Emission spectra of SiO_2/MQDs in buffer, (c) schematic of BAM/SiO_2/MQDs for bio-labeling, and (d) structure of BAM.

thermally driven spin reversals over an anisotropy energy barrier, $E_{ani}=K_{eff}\,V$, where V is the volume of the particle and K_{eff} is the effective magnetic anisotropy density. For magnetically isolated particles with uniaxial magnetic anisotropy, the spin relaxation time τ_s follows the Arrhenius equation first proposed by Néel [43],

$$\tau_s = \tau_0 \exp(K_{eff} V / k_B T) \quad (1)$$

where τ_0 is a constant characteristic of the material (on the order of 10^{-9} s), k_B is Boltzmann's constant, and T is temperature [44]. The presence of this anisotropy energy barrier produced the peak in the ZFC curve, and determined the blocking temperature T_B for SQUID measurements [45]. At T_B, the relaxation time τ_s equals the characteristic measurement time τ_m of the SQUID magnetometer. Assuming $\tau_0=10^{-9}$ s and $\tau_m=10$ s, and using an average Fe_2O_3 particle size of 10 nm (established from TEM micrographs), K_{eff} was estimated to be 0.9×10^4 J/m^3. This was lower than that of our recently reported SiO_2/γ-Fe_2O_3–CdSe nanocomposite with 12-nm MPs ($K_{eff}=5.1\times10^4$ J/m^3) [16]. As it is known that magnetic anisotropy density increases with decreasing particle size, the different K_{eff} value observed must reflect smaller strain and surface contributions to the effective anisotropy, probably due to the absence of silica shell. The current method of direct growth of CdSe QDs onto the surface of the MPs at elevated temperatures appeared to result in a decrease in strain anisotropy at the particles' surface, with a concomitant reduction in K_{eff} [46,47]. The magnetization values were expressed in electromagnetic units per gram of sample. The low saturation magnetization values (0.4 emu/g) were due to the presence of excess surfactants. When normalized to the γ-Fe_2O_3 content in each sample, the magnetization values in electromagnetic units per gram of γ-Fe_2O_3 were found to be higher ($\sim$26 emu/g).

Hysteresis loops recorded at various temperatures from 5 to 70 K (below and above the blocking temperature of $T_B=15$ K) are shown in Fig. 7. Magnetic behavior was only observed at temperatures below 15 K. For higher temperatures, the loops were narrow, which could be attributed to the superparamagnetic behavior of the MPs. This effect was also evident in the temperature behavior of the remnant magnetization (M_r) and the coercive field (H_c) (Fig. 8). As the temperature increased from 5 to 15 K, both M_r and H_c decreased to zero.

3.4. Optical properties of silica-coated MQDs and bio-labeling

Liz-Marzán et al. [48], Mulvaney et al. [49], Giersig et al. [50] and Nann and Mulvaney [51] have pioneered the silica coating method for metallic nanoparticles such as Au and Ag. These methods are not readily applicable to hydrophobic QDs as QDs are commonly coated with surfactants such as TOPO and HDA in the synthesis. Silanization protocols for hydrophobic QDs have been developed by Gerion et al. [52], Parak et al. [53], and Kirchner et al. [54]. Silica coating of hydrophobic semiconductors could also be conducted in a reverse microemulsion [33–35,55,56]. Our approach relied on the use of reverse microemulsion for silica coating. The surfactant interactions played a major role in getting the particles into the aqueous domains of the microemulsion. Thin SiO_2/MQDs were rendered soluble in water and buffers (Fig. 9a). The emission spectra (Fig. 9b) of SiO_2/MQDs in buffer indicated that the optical signatures were retained even after silica coating, implying the integrity of the MQDs after coating. The emission maximum ranged from 550 to 600 nm with a full-width-at-half-maximum (FWHM) of less than 40 nm, indicating the narrow size distribution of particles. The quantum yield of as-synthesized MQDs varied from 13% to 18% with an increase in emission wavelength from 550 to 600 nm. These values were significantly greater than the quantum yield of 3.2% reported for FePt–CdS MQDs in the organic growth solution [22]. The quantum yield of our SiO_2/MQDs varied from 8% to 13%.

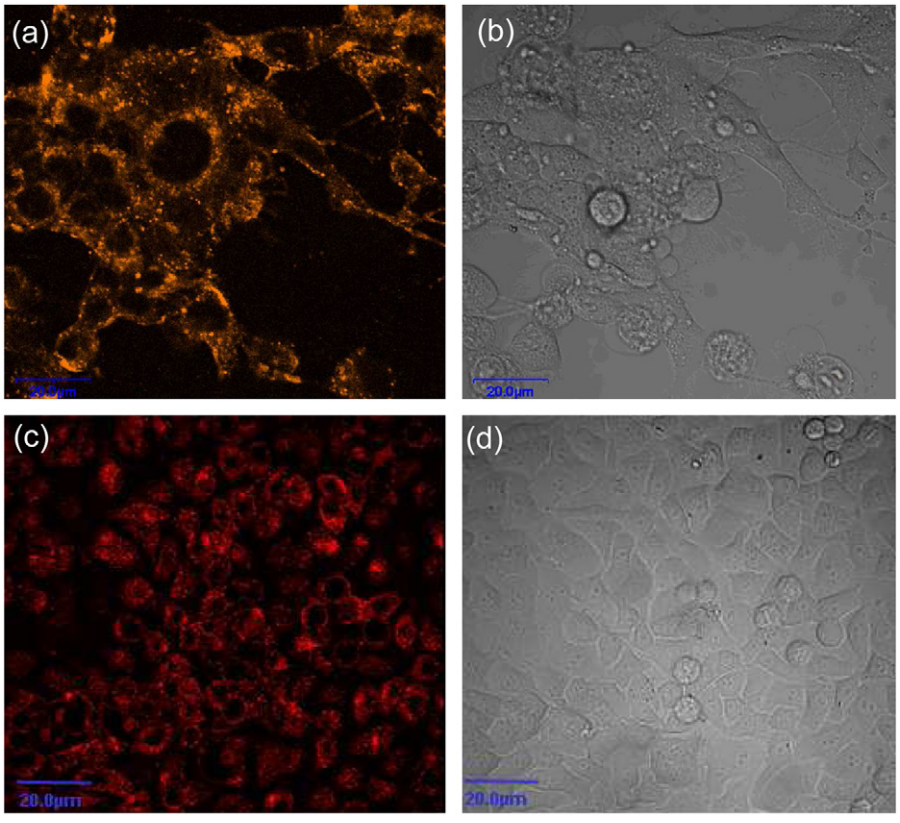

Fig. 10. (a, c) Confocal and (b, d) transmission micrographs of live cell membrane labeling of (a, b) 4T1 and (c, d) HepG2 cells using BAM/SiO_2/MQDs with (a, b) orange and (c, d) red emissions. (For interpretation of the references to color in this figure legend, the reader is referred to the web version of this article.)

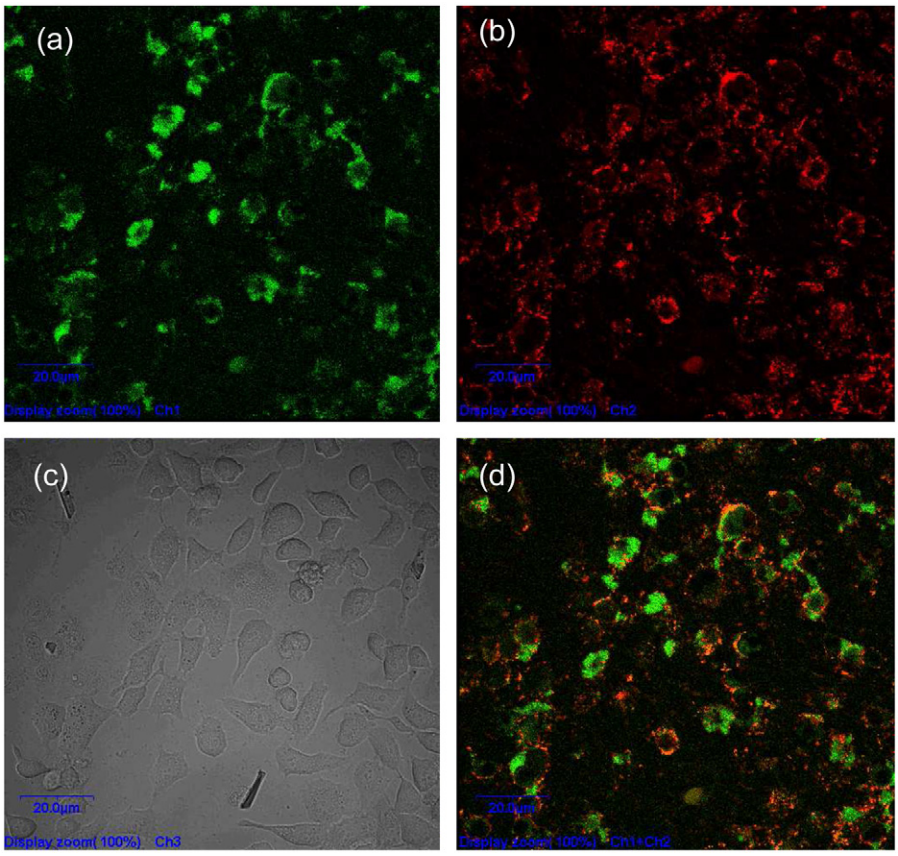

Fig. 11. (a, b, d) Confocal and (c) transmission micrographs of live cell membrane labeling of HepG2 cells using BAM/SiO_2/MQDs with green and red emissions. (For interpretation of the references to color in this figure legend, the reader is referred to the web version of this article.)

The structure of MQDs used for bio-labeling is depicted in Fig. 9c. The structure of the BAM is shown in Fig. 9d. The SiO_2/MQDs with terminal amine groups were used for bioconjugation with BAM. The reaction between amine groups (from MQDs) and NHS ester (from BAM) resulted in a covalent amide bond, exposing the oleyl groups for the effective labeling of the cell membrane of 4T1 and HepG2. CLSM [57] is commonly employed to study the imaging of cells with QDs. Typical confocal and transmission micrographs of labeled cells with conjugated MQDs are shown in Fig. 10. The BAM-functionalized SiO_2/MQDs (with orange and red emissions) labeled the outer cell membranes of 4T1 and HepG2 cancer cells. The PEG groups enhanced water solubility and reduced the non-specific adsorption of the particles. In cell biology, the cell membrane acts as the defining principle for many biological processes. Significant efforts have been devoted towards understanding the mechanisms used by cells to allow proteins, DNA, and ions to directly traverse biological membranes [58]. Fig. 11 shows the confocal and transmission micrographs of live cell membrane labeling of HepG2 cells using BAM-functionalized, silica-coated, green and red MQDs. The two-color imaging in overlay is shown in Fig. 11d.

4. Conclusion

We have demonstrated the fabrication of MQDs through a seed-mediated approach. The formation and assembly of these bi-functional nanocomposites have been elucidated by HRTEM. The MQDs exhibited superparamagnetism and tunable emissions characteristic of the components in this hybrid system. MQDs with thin silica coating were also successfully employed in the labeling of cancer cell membranes using a novel bioconjugation approach.

Acknowledgments

This work was funded by the Institute of Bioengineering and Nanotechnology (Biomedical Research Council, Agency for Science, Technology and Research, Singapore), and the National Science Foundation DMR-0604049 (at Villanova University). GCP thanks Prof. Jacques Teillet for hosting her sabbatical leave at the University of Rouen.

References

[1] D.L. Klein, R. Roth, A.K.L. Lim, A.P. Alivisatos, P.L. McEuen, Nature 389 (1997) 699–701.
[2] V.L. Klimov, A.A. Mikhailovsky, S. Xu, A. Malko, J.A. Hollingsworth, C.A. Leatherdale, H.J. Eisler, M.G. Bawendi, Science 290 (2000) 314–317.
[3] A.P. Alivisatos, W. Gu, C. Larabell, Annu. Rev. Biomed. Eng. 7 (2005) 55–76.
[4] X. Gao, L. Yang, J.A. Petros, F.F. Marshall, J.W. Simons, S. Nie, Curr. Opin. Biotechnol. 16 (2005) 63–72.
[5] I.L. Medinitz, H.T. Uyeda, E.R. Goldman, H. Mattoussi, Nat. Mater. 4 (2005) 435–446.
[6] X. Michalet, F.F. Pinaud, L.A. Bentolila, J.M. Tsay, S. Doose, J.J. Li, G. Sundaresan, A.M. Wu, S.S. Gambhir, S. Weiss, Science 307 (2005) 538–544.
[7] T. Neuberger, B. Schopf, H. Hofmann, M. Hofmann, B. von Rechenberg, J. Magn. Magn. Mater. 293 (2005) 483–496.
[8] J.M. Perez, L. Josephson, T. O'Loughlin, D. Högemann, R. Weissleder, Nat. Biotech 20 (2002) 816–820.
[9] H. Lee, E. Lee, D.K. Kim, N.K. Jang, Y.Y. Jeong, S. Jon, J. Am. Chem. Soc. 128 (2006) 7383–7389.
[10] F. Hu, L. Wei, Z. Zhou, Y. Ran, Z. Li, M. Gao, Adv. Mater. 18 (2006) 2553–2556.
[11] A.F. Thünemann, D. Schütt, L. Kaufner, U. Pison, H. Möhwald, Langmuir 22 (2006) 2351–2357.

[12] I.J.M. de Vries, W.J. Lesterhuis, J.O. Barentsz, P. Verdijk, J.H. van Krieken, O.C. Boerman, W.J.G. Oyen, J.J. Bonenkamp, J.B. Boezeman, G.J. Adema, J.W.M. Bulte, T.W.J. Scheenen, C.J.A. Punt, A. Heerschap, C.G. Figdor, Nat. Biotechnol. 23 (2005) 1407–1413.
[13] J.P. Fortin, C. Wilhelm, J. Servais, C. Ménager, J.C. Bacri, F. Gazeau, J. Am. Chem. Soc. 129 (2007) 2628–2635.
[14] N. Nasongkla, E. Bey, J. Ren, H. Ai, C. Khemtong, J.S. Guthi, S.F. Chin, A.D. Sherry, D.A. Boothman, J. Gao, Nano Lett. 6 (2006) 2427–2430.
[15] J.H. Lee, Y.M. Huh, Y.W. Jun, J.W. Seo, J.T. Jang, H.T. Song, S. Kim, E.J. Cho, H.G. Yoon, J.S. Suh, J. Cheon, Nat. Med. 13 (2007) 95–99.
[16] D.K. Yi, S.T. Selvan, S.S. Lee, G.C. Papaefthymiou, D. Kundaliya, J.Y. Ying, J. Am. Chem. Soc. 127 (2005) 4990–4991.
[17] F.X. Redl, K.S. Cho, C.B. Murray, S. O'Brien, Nature 423 (2003) 968–971.
[18] D. Wang, J. He, N. Rosenzweig, Z. Rosenzweig, Nano Lett. 4 (2004) 409–413.
[19] A.P. Alivisatos, Nat. Biotech. 22 (2004) 47–52.
[20] M. Casavola, R. Buonsanti, G. Caputo, P.D. Cozzoli, Eur. J. Inorg. Chem. 6 (2008) 837–854.
[21] L. Carbone, P.D. Cozzoli, Nano Today 5 (2010) 449–493.
[22] H. Gu, R. Zheng, X.X. Zhang, B.J. Xu, J. Am. Chem. Soc. 126 (2004) 5664–5665.
[23] K.W. Kwon, M. Shim, J. Am. Chem. Soc. 127 (2005) 10269–10275.
[24] R. Buonsanti, E. Snoeck, C. Giannini, F. Gozzo, M. Garcia-Hernandez, M.A. Garcia, R. Cingolani, P.D. Cozzoli, Phys. Chem. Chem. Phys. 11 (2009) 3680–3691.
[25] R. Buonsanti, V. Grillo, E. Carlino, C. Giannini, F. Gozzo, M. Garcia-Hernandez, M.A. Garcia, R. Cingolani, P.D. Cozzoli, J. Am. Chem. Soc. 132 (2010) 2437–2464.
[26] W. Shi, H. Zeng, Y. Sahoo, T.Y. Ohulchanskyy, Y. Ding, Z.L. Wang, P.N. Prasad, Nano Lett. 6 (2006) 875–881.
[27] T. Pellegrino, A. Fiore, E. Carlino, C. Giannini, P.D. Cozzoli, G. Ciocarella, M. Respaud, L. Palmirotta, R. Cingolani, L. Manna, J. Am. Chem. Soc. 128 (2006) 6690–6698.
[28] (a) H. Yu, M. Cen, P.M. Rice, S.X. Wang, R.L. White, S. Sun, Nano Lett. 5 (2005) 379–382;
(b) J. Jiang, H. Gu, H. Shao, E. Devlin, G.C. Papaefthymiou, J.Y. Ying, Adv. Mater. 20 (2008) 4403–4407.
[29] H.W. Gu, Z.M. Yang, J.H. Gao, C.K. Chang, B. Xu, J. Am. Chem. Soc. 127 (2005) 34–35.
[30] H. Kim, M. Achermann, L.P. Balet, J.A. Hollingsworth, V.I. Klimov, J. Am. Chem. Soc. 127 (2005) 544–546.
[31] S. Deka, A. Falqui, G. Bertoni, C. Sangregorio, G. Poneti, G. Morello, M. De Giorgi, C. Giannini, R. Cingolani, L. Manna, P.D. Cozzoli, J. Am. Chem. Soc. 131 (2009) 12817–12828.
[32] R. Di Corato, P. Piacenza, M. Musarò, R. Buonsanti, P.D. Cozzoli, M. Zambianchi, G. Barbarella, R. Cingolani, L. Manna, T. Pellegrino, Macromol. Biosci. 9 (2009) 952–958.
[33] S.T. Selvan, P.K. Patra, C.Y. Ang, J.Y. Ying, Angew. Chem. Int. Ed. 46 (2007) 2448–2452.
[34] S.T. Selvan, T.T. Tan, J.Y. Ying, Adv. Mater. 17 (2005) 1620–1625.
[35] T.T. Tan, S.T. Selvan, L. Zhao, S. Gao, J.Y. Ying, Chem. Mater. 19 (2007) 3112–3117.
[36] K. Kato, C. Itoh, T. Yasukouchi, T. Nagamune, Biotechnol. Prog. 20 (2004) 897–904.
[37] T. Hyeon, S.S. Lee, J. Park, Y. Chung, H.B. Na, J. Am. Chem. Soc. 123 (2001) 12798–12801.
[38] L. Qu, X. Peng, J. Am. Chem. Soc. 124 (2002) 2049–2055.
[39] Z.A. Peng, X. Peng, J. Am. Chem. Soc. 123 (2001) 183–184.
[40] J. Gao, W. Zhang, P. Huang, B. Zhang, X. Zhang, B. Xu, J. Am. Chem. Soc. 130 (2008) 3710–3711.
[41] G.C. Papaefthymiou, Nano Today 4 (2009) 438–447.
[42] G.C. Papaefthymiou, E. Devlin, A. Simopoulos, D.K. Yi, S.N. Riduan, S.S. Lee, J.Y. Ying, Phys. Rev. B 80 (2009) 024406-1–024406-10.
[43] L. Néel, Ann. Geophys. 5 (1949) 99–136.
[44] W.F. Brown, Phys. Rev. 130 (1963) 1677–1686.
[45] A. Aharoni, In Magnetic Properties of Fine Particles, in: J.L. Dormann, D. Fiorani (Eds.), Elsevier Science, North-Holland, 1991, pp. 3–11.
[46] B.H. Sohn, R.E. Cohen, G.C. Papaefthymiou, J. Mag. Mag. Mater. 182 (1998) 216–224.
[47] G.C. Papaefthymiou, Mater. Res. Soc. Symp. 635 (2001) C2.4.1–C2.4.7.
[48] L.M. Liz-Marzán, M. Giersig, P. Mulvaney, Langmuir 12 (1996) 4329–4335.
[49] P. Mulvaney, L.M. Liz-Marzán, M. Giersig, T. Ung, J. Mater. Chem. 10 (2000) 1259–1270.
[50] M. Giersig, T. Ung, L.M. Liz-Marzán, P. Mulvaney, Adv. Mater. 9 (1997) 570–575.
[51] T. Nann, P. Mulvaney, Angew. Chem. Int. Ed. 43 (2004) 5393–5396.
[52] D. Gerion, F. Pinaud, S.C. Williams, W.J. Parak, D. Zanchet, S. Weiss, A.P. Alivisatos, J. Phys. Chem. 105 (2001) 8861–8871.
[53] W.J. Parak, D. Gerion, D. Zanchet, A.S. Woerz, T. Pellegrino, C. Micheel, S.C. Williams, M. Seitz, R.E. Bruehl, Z. Bryant, C. Bustamante, C.R. Bertozzi, A.P. Alivisatos, Chem. Mater. 14 (2002) 2113–2119.
[54] C. Kirchner, T. Liedl, S. Kudera, T. Pellegrino, A.M. Javier, H.E. Gaub, S. Stölzle, N. Fertig, W.J. Parak, Nano Lett. 5 (2005) 331–338.
[55] M. Darbandi, R. Thomann, T. Nann, Chem. Mater. 17 (2005) 5720–5725.
[56] M. Darbandi, W. Lu, J. Fang, T. Nann, Langmuir 22 (2006) 4371–4375.
[57] K.T. Yong, J. Qian, I. Roy, H.H. Lee, E.J. Bergey, K.M. Tramposch, S. He, M.T. Swihart, A. Maitra, P.N. Prasad, Nano Lett. 7 (2007) 761–765.
[58] W. Wickner, R. Schekman, Science 310 (2005) 1452–1456.